

Note that B_{IF} is measured in cycles per second and not in radians per second, as made evident by the factor $1/2\pi$ in the formula above. The value $S_{n_c}(0)$ is often denoted as $N_0/2$, where N_0 is the noise one-sided spectral density if this is constant.

Getting back to the scheme of Figure 5.11, the additive noise process $n'(t)$ injected onto the phase error can be viewed as angular phase disturbance that replaces the narrow-band band-pass noise $n(t)$ added on the input signal when we move to the baseband model. It results [5.16]

$$\begin{aligned} n'(t) &= \frac{n_c(t)}{A} \cos \hat{\theta} + \frac{n_s(t)}{A} \sin \hat{\theta} \\ &= \frac{1}{A} \operatorname{Re}\{\vec{n}_L(t)e^{-j\hat{\theta}}\} \end{aligned} \quad (5.67)$$

In [5.16] it is shown that the statistical description of $n'(t)$ is approximately independent on the VCO output phase $\hat{\theta}(s)$, at least if the loop is locked to the input reference. Hence the sole independent variable t in the notation $n'(t)$. In other terms, the phase $\hat{\theta}(s)$ can be considered nearly constant over the short time interval $1/B_{\text{IF}}$, where a significant correlation between two noise samples $n(t)$ and $n(t+1/B_{\text{IF}})$ exists (the noise power spectrum is assumed non-zero only within the interval wide $2\pi B_{\text{IF}}$ and centred on ω_0).

Owing to the superposition principle of linear systems, to assess the effect of the input additive noise we may set $\theta = 0$ and then use n' instead of θ in Equation (5.30), to yield

$$S_{\hat{\theta}}(\omega) = |H(\omega)|^2 S_{n'}(\omega) \quad (5.68)$$

As far as the noise power is concerned, when $\theta = 0$ we have $\phi = -\hat{\theta}$ and the phase error variance (the additional phase error variance generated by the insertion of the noise $n'(t)$) is

$$\sigma_\phi^2 = \frac{1}{2\pi} \int_{-\infty}^{\infty} |H(\omega)|^2 S_{n'}(\omega) d\omega \quad (5.69)$$

In many cases of practical interest, the power spectral density of $n'(t)$ is nearly constant for all frequencies of interest (i.e., where $|H(\omega)|^2$ is significantly different from zero) and thus the following approximation can be used

$$S_{n'}(\omega) \approx \frac{S_{n_c}(0)}{A^2} = \frac{N_0}{2A^2} \quad (5.70)$$

We obtain then

$$\sigma_\phi^2 = \frac{N_0}{2A^2} \frac{1}{2\pi} \int_{-\infty}^{\infty} |H(\omega)|^2 d\omega = \frac{N_0 B_L}{A^2} \quad (5.71)$$

having defined the equivalent loop noise bandwidth

$$B_L = \frac{1}{2\pi} \int_0^{\infty} \frac{|H(\omega)|^2}{|H(0)|^2} d\omega \quad [\text{Hz}] \quad (5.72)$$

analogously to the equivalent noise bandwidth B_{IF} .

5.5.5 PLL Performance with Internal Noise Sources

The characterization of internal noise sources in a PLL is a very important topic, aiming at evaluating slave clock performance by analytical tools. Kroupa, in his paper [5.17], provided a general survey on noise properties in PLL systems.

Assuming that the noise internally generated has small amplitude and that the PLL is working locked to the reference (i.e., the input noise, if any, has small amplitude as well), the PLL can be modelled again as a linear system. Thus, a simplified version of the linear model approximating the PLL behaviour with internal noise sources is depicted in Figure 5.12. In this figure, the main noise sources are modelled as phase random processes injected as additive terms: ϕ_{VCO} [rad] is the phase noise generated by the VCO and V_{DF} [V] is the tension noise produced cumulatively by the phase detector and the loop filter. Moreover, ϕ_{in} [rad] is the phase noise on the input signal and ϕ_{out} [rad] is the overall phase noise resulting on the output signal. Please note the difference between this scheme and that of Figure 5.11: in the previous subsection, the effect of noise *added* on the input signal was analysed; in this subsection, instead, the effect of noise *modulating the phase* of signals circulating in the loop is considered.

The analysis of this linear model, by considering one input at a time among ϕ_{in} , ϕ_{VCO} and V_{DF} and owing to the superposition principle, yields the following three transfer functions (cf. Equations (5.32) and (5.33)):

$$H(s) = \frac{\phi_{\text{out}}(s)}{\phi_{\text{in}}(s)} = \frac{G_0(s)}{1 + G_0(s)} = \frac{K_0 K_d F(s)}{s + K_0 K_d F(s)} \quad (5.73)$$

$$H_A(s) = \frac{\phi_{\text{out}}(s)}{V_{\text{DF}}(s)} = \frac{H(s)}{K_d} = \frac{K_0 F(s)}{s + K_0 K_d F(s)} \quad (5.74)$$

$$H_B(s) = \frac{\phi_{\text{out}}(s)}{\phi_{\text{VCO}}(s)} = 1 - H(s) = \frac{s}{s + K_0 K_d F(s)} \quad (5.75)$$

As usual, the expression $K_0 K_d = K_0 A K_m K_1 = KA$ [s^{-1}] denotes the loop gain. Being the loop filter $F(s)$ low-pass, it is important to notice the following two basic facts.

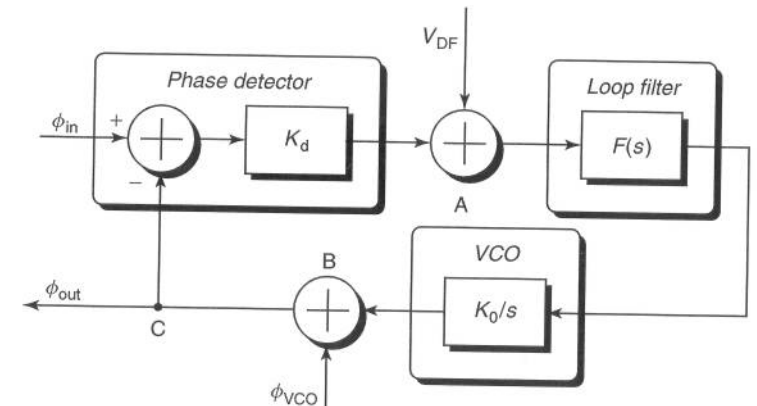


Figure 5.12. Linear model of a phase-locked loop with the main internal noise sources

- The transfer functions $H(s)$ and $H_A(s)$ are low-pass. Therefore, the phase noise on the input reference signal $s_{in}(t)$ and the internal tension noise produced by the phase detector and the loop filter are low-pass filtered to the output signal $s_{out}(t)$.
- The transfer function $H_B(s)$ is high-pass. Therefore, the internal phase noise produced by the VCO is high-pass filtered to the output signal $s_{out}(t)$.

5.5.6 Operational Ranges of Slave Clocks

Four key parameters describe the performance of a PLL in terms of operational limits of the input frequency: the *hold-in range* $\Delta\omega_{HI}$, the *pull-out range* $\Delta\omega_{PO}$, the *lock-in range* $\Delta\omega_{LI}$ and the *pull-in range* $\Delta\omega_{PI}$. Typically, we have $\Delta\omega_{LI} < \Delta\omega_{PO} < \Delta\omega_{PI} < \Delta\omega_{HI}$. Standard recommendations on slave clocks include specifications for some or all the parameters above. The definitions provided in this section are those in use in ITU-T standards on synchronization. For a more formal and mathematical treatise, the reader is referred to [5.16].

5.5.6.1 Hold-In Range

The hold-in range $\Delta\omega_{HI}$ is defined as the largest offset between the frequency ω_{in} of the input reference signal $s_{in}(t)$ and a specified nominal frequency (approximately the VCO free-run frequency ω_F), within which the slave clock maintains lock as the frequency varies slowly (rigorously speaking with $d\omega_{in}/dt \rightarrow 0$) over the frequency range.

In other terms, within the hold-in range, the PLL can track slow (*quasi-stationary*) variations of the input frequency. For this reason, the hold-in range may be called also the hold range in *static* conditions.

5.5.6.2 Pull-Out Range

The pull-out range $\Delta\omega_{PO}$ is defined as the largest offset between the input frequency ω_{in} and a specified nominal frequency (approximately the VCO free-run frequency ω_F), within which the slave clock stays in the locked mode and outside of which the slave clock cannot maintain locked mode, irrespective of the rate of the frequency change.

In other terms, within the pull-out range, the PLL can track *arbitrarily fast* variations (e.g. steps) of the input frequency. For this reason, the pull-out range may be called also the hold range in *dynamic* conditions.

5.5.6.3 Lock-In Range

The lock-in range $\Delta\omega_{LI}$ is defined as the largest offset between the input frequency ω_{in} and a specified nominal frequency (approximately the VCO free-run frequency ω_F), within which the PLL locks ‘fast’ (i.e., in a time in the order of $1/\omega_n$ seconds for a second-order PLL) to the new input frequency⁸.

5.5.6.4 Pull-In Range

The pull-in range $\Delta\omega_{PI}$ is defined as the largest offset between the input frequency ω_{in} and a specified nominal frequency (approximately the VCO free-run frequency ω_F), within

⁸ More precisely, the lock-in range is the interval within which the PLL locks to the new input frequency without *cycle slips* before settling at a stable equilibrium point. A PLL is said to slip a cycle when the phase error increases by $+2\pi$ (positive cycle slip) or -2π (negative cycle slip).

which the slave clock achieves locked mode, irrespective of how long it takes to lock⁹. The reader might be surprised that $\Delta\omega_{PI} < \Delta\omega_{HI}$. To understand this, we should consider the fundamental difference between *tracking* and *acquisition*. Tracking presumes that the PLL is already in lock and the input frequency is changed until the loop loses lock. During acquisition, the PLL is initially out of lock.

5.5.7 Operation Modes of Slave Clocks in a Synchronization Network

A slave clock may operate in the following three modes in a synchronization network, depending on the availability of a trusty reference signal at its input.

5.5.7.1 Locked Mode

The slave clock is tracking the input frequency, which keeps within the hold-in and pull-out ranges ($\omega_{in} < \Delta\omega_{PO} < \Delta\omega_{HI}$). Should the input frequency move outside the pull-out range ($\Delta\omega_{PO} < \omega_{in} < \Delta\omega_{HI}$), the slave clock stays in locked mode as well, provided that the input-frequency change rate $d\omega_{in}/dt$ is slow enough.

The locked mode may be *ideal*, if the reference signal is always available and stable, or *real* (stressed), if the reference is affected by impairments of various kind.

Even though the ideal locked mode is not typical of real synchronization network operation, understanding clock performance under ideal operation is important to get bounds for clock performance. Under ideal conditions, the slave clock operates in strict phase lock with the incoming reference. For observation intervals shorter than the PLL time constant, the clock stability is determined by the short-term stability of the local oscillator as well as by quantization effects, for example in the phase detector, if the PLL is realized with digital techniques. As it will be shown better in a later section, in the absence of input reference impairments and due to internal noise sources, the output timing signal exhibits a phase noise approximately behaving as white noise phase modulation.

Stressed operation, on the other hand, is the typical mode of operation of slave clocks receiving timing over a network facility that may introduce little impairments such as micro-interruptions. Micro-interruptions are short time intervals in which the signal becomes not usable as timing reference. In real networks, they may last tens of microseconds and can be expected even in a number of 1 to 100 per day.

All interruptions affect slave clock operation! When reference has been restored (or all the more reason if the interruption persisted and clock had to switch reference), we find some residual time error between the slave clock and the input reference, cumulating at each interruption. The actual amount of timing error produced by each reference interruption depends on the clock design, but is specified by international standards to be at worst not greater than 1 μ s. The overall timing error, sum of independent random terms, behaves as a random-walk noise phase modulation (i.e., white noise frequency modulation, as it will be shown in a later section).

Moreover, slave clocks with poor performance in response to micro-interruptions, such as some cheap clocks typically deployed at customer premises, after a reference interruption simply switch reference or enter autonomous mode of operation, producing large

⁹ Within the pull-in range, the PLL locks to the new input frequency even with one or more cycle slips. The larger the initial frequency difference, the more cycles the loop will slip before it settles. The pull-in process is also called *unaided acquisition of frequency* and is a slow and unreliable process.

phase hits on the output. This is due to the fact that most cheap clocks intended for customer premises application do not incorporate phase build-out features to limit time-keeping error on transients after micro-interruptions. The magnitude of such phase hits may be so large to make downstream clocks un-lock or switch reference and thus may cause slips in the customer network equipment.

5.5.7.2 Free-Run Mode

If the reference signal fails, or the input frequency moves outside the hold-in range (or fast outside the pull-out range) and keeps outside the pull-in range so that the clock cannot re-lock, the clock has to work *autonomously*, supplying the free-run frequency ω_F of the internal oscillator (VCO) working with null control tension. Of course, the nominal free-run frequency ω_F is designed equal to the nominal reference frequency.

Actually, real slave clocks for synchronization networks never enter plain free-run mode. Hold-over is the standard mode of autonomous operation in practical equipment.

5.5.7.3 Hold-Over Mode

As in the free-run mode, if the reference signal fails the clock works autonomously, supplying the frequency generated by the VCO. In this case, nevertheless, the last control tension value at the input of the VCO before the reference failure is maintained, so to hold the last output frequency value over. More sophisticated clocks even store several samples of the VCO control tension, so that after entering the hold-over mode the VCO is controlled with a variable tension extrapolated from the last data. An excellent hold-over stability can be achieved in this way, even under a substantial non-linear drift of the VCO frequency.

Hold-over mode is thus the slave-clock mode of operation in the rare cases that all input references failed or are judged not reliable (for example, because providing an input frequency outside the pull-in range). Hold-over performance is mainly characterized by the residual initial frequency offset and frequency drift. The initial frequency offset is caused by the setability resolution of the local oscillator frequency and the noise on the timing reference on clock un-locking. Frequency drift is due to ageing of the local oscillator.

5.6 FREQUENCY-DOMAIN AND TIME-DOMAIN STABILITY CHARACTERIZATION

The characterization of clock stability is usually carried out by characterizing, by means of suitable analytical tools, the random processes $\varphi(t)$, $x(t)$, $\text{TE}(t)$, $y(t)$ or $v(t)$ (cf. Equations (5.4)(5.11)(5.13)). There is a huge literature on time and frequency stability characterization for precision oscillators. An essential list of selected publications on this subject is reported in the bibliography [5.1]–[5.4][5.18]–[5.33].

Historically, a dichotomy between the characterization of such processes in the *Fourier-frequency domain* and in the *time domain* were established: the inadequacy of measurement equipment strengthened the barriers between these two characterizations of the same noise process. Although these barriers are mainly artificial, nevertheless it is not always possible to translate unambiguously from any quantity of one domain to anyone of the other.

Examples of stability measures in the frequency domain are the one-sided *Power Spectral Densities* (PSDs, or more simply spectra) of the phase, time and frequency fluctuations, since they are functions of the Fourier frequency f .

Note that the word ‘frequency’ may be used with two different meanings that should not be confused. The symbol $v(t)$ denotes the time-dependent instantaneous frequency of the clock. The symbol f indicates the time-independent Fourier frequency that is argument of spectral densities and Fourier transforms: in base-band representation, positive values of f denote frequencies above the central frequency v_n , negative values denote frequencies below v_n .

On the other hand, variances of the same fluctuations, averaged over a given observation interval, are examples of stability measures in the time domain, since they are functions of the observation interval τ (time).

In general, both frequency-domain and time-domain stability measures can be evaluated starting from samples of time error or of instantaneous frequency.

5.7 CLOCK STABILITY CHARACTERIZATION IN THE FREQUENCY DOMAIN

Analysis in the Fourier frequency domain is of great importance both for theoretical purposes, in terms of richness of information included, and for practical application purposes, since it expresses the power spreading in the frequency domain around the ideal carrier frequency. For this reason, spectral densities of various kinds have been widely used for clock stability characterization.

In particular, the analogue measurement of PSD functions directly in the frequency domain (spectral analysis) has been for a long time the main technique for studying the behaviour of oscillators.

More recently, the introduction of high-resolution digital instrumentation for the measurement in the time domain (time counters) made more appealing the time-domain measures in most applications. In fact, the recent telecommunications standards recommend, as standard stability measures, time-domain quantities evaluated from samples of time error measured directly in the time domain.

However, spectral analysis [5.34] of clock noise is still considered one of the main tools for clock characterization [5.1][5.2][5.4][5.25][5.27]. Nowadays, digital spectral analysers evaluate the PSD of interest by Fast Fourier Transform (FFT) computation on data samples measured in the time domain by a time counter.

5.7.1 Power Spectral Density of the Timing Signal

The most straightforward and intuitive way to characterize the accuracy and stability of the timing signal $s(t)$ supplied by a clock is to evaluate directly its two-sided PSD, or more precisely its low-pass (base-band) representation, often denoted as $S_s^{\text{RF}}(f)$ (spectrum in radio frequency).

The RF spectrum $S_s^{\text{RF}}(f)$ is a continuous function, proportional to the timing-signal power delivered to a matched load per unit of bandwidth centred on f . It is measured in [W/Hz] or [V²/Hz] units.

In case of ideal timing signal (constant frequency $v(t) = v_n$), the radio-frequency (RF) spectrum $S_s^{\text{RF}}(f)$ is a Dirac pulse $P_s \delta(f)$, where P_s is the signal power, as shown in

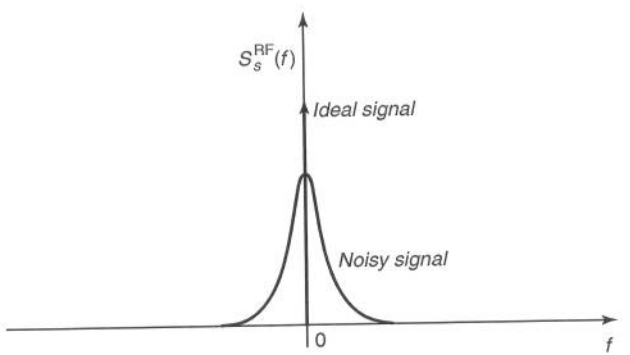


Figure 5.13. Power spectral density of ideal and noisy timing signals

Figure 5.13. In the real case of timing signal affected by some phase and amplitude noise, the PSD ideal pulse spreads and exhibits some spectral content also at frequencies $f \neq 0$. A *pedestal* around the ideal frequency $f = 0$, therefore, is typically found in power spectral densities measured on real oscillators.

The spectrum $S_s^{\text{RF}}(f)$ is definitely *not* a good tool to characterize clock frequency stability: unfortunately, given $S_s^{\text{RF}}(f)$, it is not possible to determine unambiguously whether the power at various Fourier frequencies is the result of amplitude rather than phase fluctuations in the timing signal $s(t)$. Nevertheless, if the power due to amplitude modulation noise is negligible and the phase fluctuations are small (i.e., the mean square value $\langle \varphi^2(t) \rangle^{10}$ is much less than 1 rad^2) as it happens in practical clocks, then the spectrum $S_s^{\text{RF}}(f)$ has approximately the same *shape* of the phase-noise spectrum $S_\varphi(f)$. However, it is still difficult to obtain quantitative results about $\varphi(t)$ from it.

5.7.2 Power Spectral Densities of Phase and Frequency Fluctuations

In the Fourier frequency domain, the most commonly used stability measures are the one-sided PSDs of $\varphi(t)$, $x(t)$ and $y(t)$ denoted as $S_\varphi(f)$ [rad^2/Hz], $S_x(f)$ [ns^2/Hz] and $S_y(f)$ [Hz^{-1}] respectively, because they describe directly the time and frequency stability characteristics.

The PSDs above are equivalent representations of the same noise process. In fact, the following relationships hold among them:

$$\begin{aligned} S_y(f) &= \frac{f^2}{v_n^2} S_\varphi(f) \\ S_x(f) &= \frac{S_\varphi(f)}{(2\pi v_n)^2} \\ S_y(f) &= (2\pi f)^2 S_x(f) \end{aligned} \quad (5.76)$$

¹⁰ The symbol $\langle \cdot \rangle$ denotes the infinite *time-average operator* on the argument function. For example, in the case of continuous-time argument function $s(t)$, it is defined as

$$\langle s(t) \rangle = \lim_{T \rightarrow \infty} \frac{1}{2T} \int_{-T}^T s(t) dt$$

The PSD $S_y(f)$ was first recommended in 1971 by IEEE as standard frequency stability measure in the Fourier frequency domain [5.1][5.7]. It is worthwhile noticing that, under the assumption of Gaussian stationary random processes, the power spectral density (or equivalently the autocorrelation function, which is its inverse Fourier transform) contains maximum information about the random process. The time-domain variances that will be defined in the next sections are related to the spectral density, by some integral relationships, but do not include full characterization of the process.

Spectral densities of phase and frequency fluctuations, in principle, can be measured by a spectrum analyser following some kind of phase and frequency demodulator.

5.7.3 Other Spectral Measures

The other two spectral measures of phase and frequency stability that are sometimes encountered are the PSD of non-normalized frequency fluctuations $\Delta v(t)$ ¹¹

$$S_{\Delta v}(f) = v_n^2 S_y(f) \quad (5.77)$$

measured in [Hz^2/Hz], and the single-sideband measure of phase noise

$$\mathcal{L}(f) = \frac{1}{2} S_\varphi(f) \quad (5.78)$$

(read as *script 'ell'*) valid only for values of the Fourier frequency far enough from the carrier at $f = 0$, or more precisely in the interval $f_A < f < \infty$ where

$$\int_{f_A}^{\infty} S_\varphi(f) df \ll 1 \text{ rad}^2 \quad (5.79)$$

The quantity $\mathcal{L}(f)$ is usually measured in [dBc/Hz] units (decibel of carrier-over-noise power per bandwidth unit), as

$$\mathcal{L}(f) \Big|_{\frac{\text{dBc}}{\text{Hz}}} = 10 \log_{10} \mathcal{L}(f) \quad (5.80)$$

This quantity is found rather commonly in technical specifications of commercial oscillators. The reason of its appeal lies in the physical interpretation of $\mathcal{L}(f)$: a signal-to-noise ratio that can be assessed readily on a spectrum analyser. Its use is not recommended by relevant standards.

5.8 CLOCK STABILITY CHARACTERIZATION IN THE TIME DOMAIN

While frequency-domain characterization proves to be very meaningful and complete in studying the behaviour of oscillators, it is important to point out that the main concern in digital telecommunications lies in controlling time deviations *over given observation intervals*. For example, the buffer-fill level in digital transmission and switching equipment

¹¹ Unfortunately, there is a lack of uniformity in the notation among authors. The symbol $\Delta v(t)$ used herein should not be confused with the symbol Δv used in Equation (5.4), denoting the time-constant starting frequency offset of the clock. In Equation (5.4), the symbol $\Delta v(t)$ was denoted as $v_a(t)$.

is proportional to the time error cumulated between the write and read clocks. Controlling the time error over a certain observation interval means to control buffer overflows and underflows over time intervals of that length.

Time-domain characterization of time and frequency stability answers the obvious question: what is the stability (i.e., time and frequency deviation) of the timing signal under test over a given time interval τ (determined by the particular field of application)? Time-domain stability quantities are basically a sort of prediction of the expected time and frequency deviations over an observation interval τ . Therefore, they are more oriented to telecommunications purposes than spectral densities. Moreover, time-domain analysis is often much more efficient in providing meaningful measures of long-term performance.

Instabilities in oscillators are time variations of the quantities of interest (i.e., phase and frequency). Time-domain characterization is thus based on the measure of variations that occur over a specified time interval τ . Since phase and frequency of real oscillators are random phenomena, measurement must involve some time-averaging to yield statistically meaningful quantities.

In the following, the most important time-domain stability quantities defined in literature are presented. For each of them, the theoretical definition is given. Finally, the standard estimators of the time-domain quantities defined by ITU-T and ETSI, for the specification of timing interface requirements, are provided in the last subsection.

Among the list of publications already cited, for a general but thorough scientific treatise on time-domain quantities we recommend especially the excellent survey papers [5.1][5.2][5.22]. The third one, in particular, provides an outstanding review, for both breadth and depth, of quantities defined for time and frequency stability characterization. Other fundamental papers for time-domain characterization are, amongst all, [5.3][5.4][5.20][5.21][5.26][5.28]. Finally, papers [5.31][5.32][5.33] focus on characterization and measurement of telecommunications clocks.

5.8.1 Basic Measurement of $y(t)$ in the Time Domain

The oscillator *instantaneous* frequency $v(t)$ and fractional frequency $y(t)$, defined in Equations (5.4) and (5.11) respectively, are not actually observable in practice, because any frequency measurement technique does involve a finite time interval over which the frequency is measured and averaged, for example by counting the number of cycles of the input signal during the time interval.

Therefore, the average value of the frequency, measured over an observation interval τ beginning at a generic instant t_k , is a quantity more directly related to the experimental result. In particular, the averaged sample of the normalized, fractional frequency $y(t)$ is very widely used. It is defined as [5.1][5.22]

$$\bar{y}_k(\tau) = \langle y(t_k) \rangle_\tau = \frac{1}{\tau} \int_{t_k}^{t_k + \tau} y(t) dt \quad (5.81)$$

From Equation (5.11), we get moreover

$$\bar{y}_k(\tau) = \frac{\varphi(t_k + \tau) - \varphi(t_k)}{2\pi v_n \tau} = \frac{x(t_k + \tau) - x(t_k)}{\tau} \quad (5.82)$$

It is worthwhile remarking, at this point, that the operator in the discrete-time domain that corresponds to the derivative operator defined in the continuous-time domain is the

difference operator. The first difference y_k of a sequence of samples $\{x_k\}$, evenly spaced with sampling period T , is given by

$$1^{\text{st}} \text{ difference : } y_k = \frac{x_{k+1} - x_k}{T} \quad (5.83)$$

equivalent in the discrete-time domain to the first derivative $y(t) = x'(t)$ in the continuous-time domain. Analogously, the second difference z_k is given by

$$2^{\text{nd}} \text{ difference : } z_k = \frac{y_{k+1} - y_k}{T} = \frac{x_{k+2} - 2x_{k+1} + x_k}{T^2} \quad (5.84)$$

equivalent to the second derivative $z(t) = y'(t) = x''(t)$. Further-order differences are defined similarly.

The quantity \bar{y}_k is easily related to experimental results, produced for example by time-counting techniques. Thus, it has been used to define most time-domain quantities that will be presented in the following. One sample \bar{y}_k is given by one single measurement of duration τ accomplished starting at time t_k . Right now, it is worthwhile noticing that several samples \bar{y}_k , given by repeated measurements, are needed to allow statistical characterization of instability over the time interval τ .

Due to random fluctuations of $y(t)$ in real oscillators, repeated measurements of \bar{y}_k yield random results (or better, different samples of a random variable). The fundamental issue of time and frequency characterization in the time domain is thus to identify suitable statistical measures of \bar{y}_k . In particular, a statistical measure of the dispersion of the \bar{y}_k samples provides a time-domain measure of instability over τ .

5.8.2 Classical Variance of $y(t)$ (True Variance)

The plain, classical variance σ^2 and its square root σ (standard deviation) are widely used statistical tools to measure the dispersion of samples of a random variable. In our case, under the assumption that $y(t)$ is ergodic and has zero mean, the variance is simply equal to

$$\sigma^2[\bar{y}_k] = \langle \bar{y}_k^2 \rangle = I^2(\tau) \quad (5.85)$$

This quantity is a theoretical measure and is also referred to as *true variance*, as based on averaging an infinite number of samples. It is also denoted as $I^2(\tau)$, because it indicates that it is a measure of *instability* over the time interval τ .

For *stationary* frequency fluctuations, the true variance has the following limit values:

$$\begin{aligned} \lim_{\tau \rightarrow 0} I(\tau) &= \sqrt{\langle y^2(t) \rangle} \\ \lim_{\tau \rightarrow \infty} I(\tau) &= 0 \end{aligned} \quad (5.86)$$

In other words, for $\tau \rightarrow 0$ we approach ideal instantaneous frequency measurement (yielding the root mean square value of $y(t)$) and for $\tau \rightarrow \infty$ stationary fluctuations tend to be completely averaged out.

Despite its mathematical simplicity, the true variance $I^2(\tau)$ is really not a useful tool for clock stability characterization, because its time-averaging does not converge for some common kinds of phase noise, such as flicker and random-walk frequency noise (see Section 5.9 for common types of clock noise). In particular, the limit value

for $\tau \rightarrow \infty$ may approach infinity in such cases. Therefore, more suitable quantities for clock stability characterization, based on the concept of sample variance, were introduced beginning from 1966 by Allan [5.3] and others to cope with such convergence issues in most cases of practical interest.

5.8.3 M-Sample Variance of $y(t)$

The *M-sample variance* is based upon averaging an ensemble of a *finite* number M of samples \bar{y}_k ($k = 1, 2, \dots, M$) defined as previously: each sample \bar{y}_k is measured over an observation interval τ beginning at instant t_k . Sampling times are evenly spaced $T : t_{k+1} = t_k + T$. Thus, the dead time between measurements is $T - \tau$.

The *M-sample variance* may be defined in several possible ways, consisting in biased or unbiased estimates of the true variance (5.85) as described in [5.22]. Rutman suggested [5.2] as the main estimate of the average of M samples the definition

$$\sigma_y^2(M, T, \tau) = \frac{1}{M-1} \sum_{i=1}^M \left(\bar{y}_i - \frac{1}{M} \sum_{j=1}^M \bar{y}_j \right)^2 \quad (5.87)$$

This quantity is a random variable itself and its infinite time-average can be used as a measure of frequency stability over a time interval τ . In particular, for $\tau = T$ and white frequency noise (see Section 5.9 for noise types) the definition above is an unbiased estimate of the true variance, as

$$\langle \sigma_y^2(M, T, \tau) \rangle = I^2(\tau) \quad (5.88)$$

Equation (5.87) estimates the mean squared deviation of M samples of \bar{y}_k from their mean value, as recommended by any good statistics textbook. There is a long story about why the denominator is $M - 1$ instead of the more obvious M . Actually, this denominator is found also for any stationary noises when T is much longer than the correlation time of $y(t)$ (i.e., when the samples \bar{y}_k are independent)¹².

5.8.4 Allan Variance

To allow standard adoption of a unique time-domain measure that can be used unambiguously in all laboratories, the IEEE subcommittee on frequency stability recommended in 1971 [5.1][5.7] the use of the sample variance with $M = 2$ and adjacent samples with zero dead time (i.e., $T = \tau$), following the pioneering work of Allan in 1966 [5.3].

The resulting measure owes its name to its inventor and is thus known as *Allan variance*, defined as

$$\langle \sigma_y^2(2, \tau, \tau) \rangle = \left\langle \sum_{i=1}^2 \left(\bar{y}_i - \frac{1}{2} \sum_{j=1}^2 \bar{y}_j \right)^2 \right\rangle \quad (5.89)$$

¹² As noticed in the excellent book on numerical computing [5.35], which we definitely recommend, the $M - 1$ denominator *should* be changed to M if you ever are in the pleasant situation of measuring the variance of a distribution whose mean is known *a priori*, rather than being estimated from the data measured. By the way, the authors of [5.35] opportunely comment also that, if the difference between $M - 1$ and M ever matters to you, then you are probably up to no good anyway (for example, trying to substantiate a questionable hypothesis with marginal data).

With more compact notation, the definition of the Allan variance is usually written as

$$\sigma_y^2(\tau) = \frac{1}{2} \langle (\bar{y}_{k+1} - \bar{y}_k)^2 \rangle \quad (5.90)$$

The Allan variance is also known as *two-sample variance*, since pairs of adjacent measurements are grouped together.

The Allan variance too is a theoretical measure, as based on averaging an infinite number of samples. However, it has much greater practical utility than $I^2(\tau)$, because it converges for all kinds of power-law noise (see Section 5.9 for noise types).

From Equation (5.82), the Allan variance definition can also be written as time-average of the second difference of phase or time error samples

$$\sigma_y^2(\tau) = \frac{1}{2\tau^2} \langle [x(t_k + 2\tau) - 2x(t_k + \tau) + x(t_k)]^2 \rangle \quad (5.91)$$

To summarize, Allan variance computation is based on time-averaging combinations of pairs of frequency samples or of triplets of time samples.

Experimentally, only estimates of $\sigma_y^2(\tau)$ can be obtained from a finite number of samples \bar{y}_k , taken over a finite duration. Therefore, an inherent statistical uncertainty (usually plotted as error bars) exists when a finite number N of values of \bar{y}_k is used to estimate $\sigma_y^2(\tau)$. A widely used estimator (adopted also by international telecommunications standard bodies, as shown in a later section) is

$$\sigma_y^2(\tau, N) = \frac{1}{2(N-1)} \sum_{i=1}^{N-1} (\bar{y}_{i+1} - \bar{y}_i)^2 \quad (5.92)$$

This quantity is itself a random variable, whose variance (i.e., the variance of the estimated variance) may be used to assess the error bars on the plot of $\sigma_y^2(\tau)$ versus τ [5.20][5.29]. For long-term measurements, the size of N is severely limited by the overall measurement duration. In general, along a plot of $\sigma_y^2(\tau)$ versus τ , error bars are negligible at the left (short τ) and large at the right (long τ).

5.8.5 Modified Allan Variance

The relatively poor discrimination capability of the Allan variance against white and flicker phase noise, as it will be shown in Section 5.10, prompted the development of the so-called *modified Allan variance* in 1981 [5.24][5.26][5.28], defined as

$$\begin{aligned} \text{Mod } \sigma_y^2(n\tau_0) &= \frac{1}{2} \left\langle \left[\frac{1}{n} \sum_{i=1}^n (\bar{y}_{i+n} - \bar{y}_i) \right]^2 \right\rangle \\ &= \frac{1}{2n^2\tau_0^2} \left\langle \left[\frac{1}{n} \sum_{j=1}^n (x_{j+2n} - 2x_{j+n} + x_j) \right]^2 \right\rangle \end{aligned} \quad (5.93)$$

where τ_0 is the sampling period (previously denoted as T in the definition of the *M-sample variance*), the observation interval is given by $\tau = n\tau_0$ and the samples of the random time deviation $x(t_k)$ are simply denoted as x_k .

To summarize, modified Allan variance differs from basic Allan variance in the additional average over n adjacent measurements. From the definition above, moreover, it is evident that for $n = 1$ ($\tau = \tau_0$) the modified Allan variance coincides with the Allan variance.

5.8.6 Time Variance (TVAR)

The Allan variance and the modified Allan variance are measures of the stability of the fractional frequency and thus they are a-dimensional. More recently, an additional variance, closely related to the modified Allan variance, was introduced aiming at measuring directly time stability: the *Time variance*, better known with its abbreviated name TVAR [5.28]. It is defined as

$$\sigma_x^2(\tau) = \frac{\tau^2}{3} \text{Mod } \sigma_y^2(\tau) \quad (5.94)$$

with dimension [time²].

The TVAR has been widely adopted by telecommunications international standards for the specification of timing interfaces.

5.8.7 Root Mean Square of the Time Interval Error (TIE_{rms})

The root mean square value of the TIE is formally defined as

$$\text{TIE}_{\text{rms}}(t; \tau) = \sqrt{\mathbb{E}\{[\text{TE}(t + \tau) - \text{TE}(t)]^2\}} \quad (5.95)$$

with dimension [time], where the operator $\mathbb{E}\{\cdot\}$ (*expectation operator*) denotes *ensemble-averaging*¹³. Under the assumption of ergodic processes, the ensemble-average above is equal to infinite time-average and does not depend on the time t . Thus, this quantity can be denoted shortly as $\text{TIE}_{\text{rms}}(\tau)$.

Experimentally, a simple estimate of $\text{TIE}_{\text{rms}}(\tau)$ can be obtained from a finite number N of samples $\text{TE}_k = \text{TE}(t_k)$, taken over a finite duration, as

$$\text{TIE}_{\text{rms}}(n\tau_0) = \sqrt{\frac{1}{N-n} \sum_{i=1}^{N-n} (\text{TE}_{i+n} - \text{TE}_i)^2} \quad (5.96)$$

where $\tau = n\tau_0$, with $n = 1, 2, \dots, N-1$.

It is interesting to notice that, if in the timing signal model (5.4) the only non-ideal component is the random frequency deviation $v_a(t)$, then the TIE_{rms} is directly linked to the classical variance of $y(t)$, as

$$\text{TIE}_{\text{rms}}(\tau) = I(\tau) \cdot \tau \quad (5.97)$$

5.8.8 Maximum Time Interval Error

Recalling the definition of the Time Interval Error $\text{TIE}_t(\tau)$ (cf. Equation (5.16)), the *Maximum Time Interval Error* function $\text{MTIE}(\tau, T)$ is defined as the maximum peak-to-peak

¹³ The ensemble-averaging operation requires knowing the probability distribution of the ensemble. Under the common assumption of ergodic processes, the ensemble-average is equal to the infinite time-average (see for example [5.36]).

variation of TE in all the possible observation intervals τ ¹⁴ within a measurement period T , as

$$\text{MTIE}(\tau, T) = \max_{0 \leq t_0 \leq T-\tau} \left\{ \max_{t_0 \leq t \leq t_0+\tau} [\text{TE}(t)] - \min_{t_0 \leq t \leq t_0+\tau} [\text{TE}(t)] \right\} \quad (5.98)$$

The sample plot in Figure 5.14, especially if compared to Figure 5.2, clarifies the meaning of $\text{MTIE}(\tau, T)$ and its relationship with $\text{TIE}(\tau)$.

It should be noted, however, that the standards in force specify the MTIE limits simply as a function of τ (or S), thus implicitly assuming

$$\text{MTIE}(\tau) = \lim_{T \rightarrow \infty} \text{MTIE}(\tau, T) \quad (5.99)$$

In other words, to rigorously assert the MTIE compliance of a clock with standard specifications, one should verify that, for every τ , $\text{MTIE}(\tau)$ stays below the allowed limits *for all the device life*. As an extreme case, if after years of regular operation a clock should exhibit a fortuitous over-mask phase hit, this event would cancel all the past (honest) history in the resulting MTIE curve.

Now, if phase fluctuations were modelled ideally by a Gaussian probability distribution of the amplitudes (this assumption has been somehow verified experimentally, especially under white phase noise [5.20]), the maximum range spanned by TE might reach infinitely large values. Increasing the measurement period T allows to observe the tails of the distribution: they are less likely but, at least in principle, unlimited.

Therefore, the measured value $\text{MTIE}(\tau, T)$ depends in general not only on τ but also, to a smaller extent, on the overall period T during which the clock has been under test.

It is clear that a single measurement of $\text{MTIE}(\tau, T)$, on one realization of the $\text{TE}(t)$ random process and based on one measurement period T , yields a random variable result of that particular experiment. Therefore, alone, it is not adequate for a rigorous characterization of the oscillator under test.

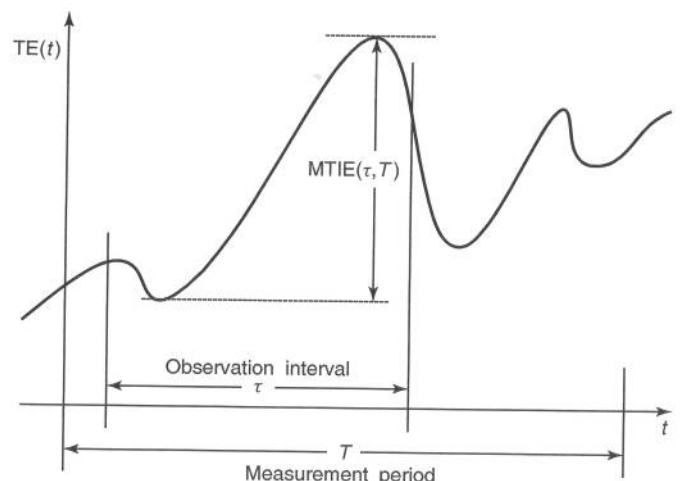


Figure 5.14. Definition of $\text{MTIE}(\tau, T)$

¹⁴ In early ITU-T Recommendations [5.37] and in ANSI standards [5.38], the observation interval τ is denoted with S .

In order to cope with these issues, ITU-T [5.39] redefined the quantity MTIE(τ, T) as a specified percentile β of the random variable X result of a single measurement of MTIE(τ, T), i.e. (cf. Equation (5.98))

$$X = \max_{0 \leq t_0 \leq T-\tau} \left\{ \max_{t_0 \leq t \leq t_0+\tau} [\text{TE}(t)] - \min_{t_0 \leq t \leq t_0+\tau} [\text{TE}(t)] \right\} \quad (5.100)$$

Based on such a definition, therefore, a MTIE β -percentile mask

$$\text{MTIE}_{\beta-\text{perc}}(\tau) \leq a_\beta(\tau) \quad (5.101)$$

gives the limit $a_\beta(\tau)$ not to be exceeded in more than a $1 - \beta$ fraction of measurements, for any T .

ITU-T Rec. G.810 [5.39] suggests also an expression to estimate the β -percentile range from multiple range measures. Let X_1, X_2, \dots, X_M be a set of single independent samples of MTIE(τ, T), measured according to Equation (5.100) on M measurement periods and sorted in ascending order, i.e. $X_1 \leq X_2 \leq \dots \leq X_M$. Let x_β be the β -percentile of the random variable X . Then, a confidence interval for x_β , expressed as the probability that x_β falls between the samples X_r and X_s (with $r < s$), is given by

$$P\{X_r \leq x_\beta \leq X_s\} = \sum_{k=r}^{s-1} \frac{M!}{k!(M-k)!} \beta^k (1-\beta)^{M-k} \quad (5.102)$$

The MTIE has been widely adopted in telecommunications international standards for the specification of timing interfaces, even before TVAR since the 1980s. Actually, it was defined aiming directly at buffer size design in bit synchronizers. Recalling that described in Section 2.3.2, bit synchronization is accomplished by writing the bits of the asynchronous bit stream into an elastic store (buffer) at their own instantaneous arrival rate f_w and by reading them out with the frequency f_r of the equipment local clock. The elastic store absorbs limited random zero-mean frequency fluctuations between the write and read clocks. Nevertheless, larger fluctuations or any frequency offset $|f_w - f_r|$ will make the buffer empty or overflow sooner or later. If the buffer empties, some bytes are repeated in transmission; if the buffer overflows, some are lost. Such events are called *slips*. A larger buffer size allows reducing the slip rate, for any given clock accuracy.

Now, it is important to point out that in elastic stores the buffer-fill level is proportional to the TE between the input digital signal and the local equipment clock. Therefore, ensuring the clock compliance with timing specifications given in terms of MTIE guarantees that certain buffer thresholds are never exceeded. If MTIE limits are low enough, this may mean that no slips or pointer justifications should ever take place. This fact accounts for MTIE's appeal in supporting the design of equipment buffer size.

Papers [5.33][5.40][5.41] deal with specific topics about MTIE and its measurement. Moreover, a section in Chapter 7 is specifically devoted to MTIE practical measurement issues.

5.8.9 Standard Estimators of Stability Quantities Defined in ITU-T Recommendations and ETSI Standards

Among the several quantities defined in literature for characterizing time and frequency stability, the following five in the time domain have been considered by

ITU-T and ETSI standard bodies [5.39][5.42] for the specification of timing interface requirements:

- the *Allan Deviation* (ADEV) $\sigma_y(\tau)$, square root of the Allan Variance (AVAR) (5.90);
- the *Modified Allan Deviation* (MADEV) mod $\sigma_y(\tau)$, square root of the Modified Allan Variance (MAVAR) (5.93);
- the *Time Deviation* (TDEV) $\sigma_x(\tau)$, square root of the Time Variance (TVAR) (5.94);
- the *root mean square of Time Interval Error* (TIE_{rms}) (5.95);
- the *Maximum Time Interval Error* (MTIE) (5.98).

Actually, while TIE_{rms} and MTIE have been defined based on the TE process, ADEV, MADEV and TDEV are theoretically defined in terms of the $x(t)$ process (5.11), i.e. of the random time deviation stripped of the deterministic components. Nevertheless, in order to overcome the complex problem of removing the frequency offset and drift from the TE measured data—and to achieve uniformity in the evaluation procedure of all the five standard stability quantities—the international telecommunication standards bodies simply recommend the use of TE(t) samples instead of $x(t)$ samples also for ADEV, MADEV and TDEV measurements. This choice is well justified based on the following:

- ADEV, MADEV and TDEV are not sensitive to any constant frequency offset in the TE data (they are based on a second difference operator, analogous in the discrete-time domain to the second derivative in the continuous-time domain);
- the frequency drift contribution is usually negligible in the observation intervals of interest in telecommunications ($\tau < 10^4$ s);
- the concern is not to rigorously characterize the noise types affecting the clock under test, but simply to limit the overall time deviations to the purposes of network design.

Therefore, to the practical purposes of telecommunications clock stability measurement, the processes TE(t) (5.13) and $x(t)$ (5.11) are considered synonymous. The Time Error samples TE(t_k) are referred to simply as $x(t_k)$. In conclusion, based on a sequence of N TE samples, defined as

$$x_k = x(t_0 + (k-1)\tau_0) \quad \text{for } k = 1, 2, \dots, N \quad (5.103)$$

i.e. measured with sampling period τ_0 over a measurement interval $T = (N-1)\tau_0$ and starting at an initial observation time t_0 , the following five standard estimators have been defined by the ITU-T [5.39] and ETSI [5.42] bodies:

$$\text{ADEV}(\tau) = \sqrt{\frac{1}{2n^2\tau_0^2(N-2n)} \sum_{i=1}^{N-2n} (x_{i+2n} - 2x_{i+n} + x_i)^2} \quad \text{for } n = 1, 2, \dots, \left\lfloor \frac{N-1}{2} \right\rfloor \quad (5.104)$$

$$\text{MADEV}(\tau) = \sqrt{\frac{1}{2n^4\tau_0^2(N-3n+1)} \sum_{j=1}^{N-3n+1} \left[\sum_{i=j}^{n+j-1} (x_{i+2n} - 2x_{i+n} + x_i) \right]^2} \quad \text{for } n = 1, 2, \dots, \left\lfloor \frac{N}{3} \right\rfloor \quad (5.105)$$

$$\text{TDEV}(\tau) = \sqrt{\frac{1}{6n^2(N-3n+1)} \sum_{j=1}^{N-3n+1} \left[\sum_{i=j}^{n+j-1} (x_{i+2n} - 2x_{i+n} + x_i) \right]^2} \quad \text{for } n = 1, 2, \dots, \left\lfloor \frac{N}{3} \right\rfloor \quad (5.106)$$

$$\text{TIE}_{\text{rms}}(\tau) = \sqrt{\frac{1}{N-n} \sum_{i=1}^{N-n} (x_{i+n} - x_i)^2} \quad \text{for } n = 1, 2, \dots, N-1 \quad (5.107)$$

$$\text{MTIE}(\tau) = \max_{1 \leq k \leq N-n} \left[\max_{k \leq i \leq k+n} x_i - \min_{k \leq i \leq k+n} x_i \right] \quad \text{for } n = 1, 2, \dots, N-1 \quad (5.108)$$

where $\tau = n\tau_0$ is the observation interval and $\lfloor z \rfloor$ denotes ‘the greatest integer not exceeding z ’.

Actually, most standard specifications are based on just two quantities among the five adopted: TVAR and MTIE. In Appendices 5A and 5B, efficient algorithms for fast computation of the TVAR and MTIE estimators are provided.

5.8.10 Translation from Frequency-Domain to Time-Domain Measures

Studying the translation relationships between stability quantities defined in the Fourier-frequency domain and in the time domain is interesting for several reasons [5.22]:

- relationships found provide a unified picture of frequency stability characterization;
- power-law noise types identified in the frequency domain (see Section 5.9) may be characterized by specific laws on the trends of time-domain quantities;
- stability measurements sometimes can be made only in one domain, due to equipment availability or capability; such relationships between quantities can then give an estimate of the performance in the other domain.

The translation between quantities in the two domains can be made by defining a suitable *transfer function* associated to each time-domain quantity [5.22]. Then, any time-domain quantity can be obtained by *integrating the noise spectral density filtered by the characteristic transfer function*, as it will be shown in the following. These relationships found are thus called *integral relationships*.

5.8.10.1 True Variance of $y(t)$

First, we notice that the true variance $I^2(\tau)$ (5.85) (assuming that $y(t)$ is zero-mean) can be written as

$$\begin{aligned} I^2(\tau) &= \langle \bar{y}_k^2 \rangle = \left\langle \left[\frac{1}{\tau} \int_{t_k}^{t_k+\tau} y(t) dt \right]^2 \right\rangle \\ &= \left\langle \left[\int_{-\infty}^{\infty} y(t) h_I(t_k - t) dt \right]^2 \right\rangle = \langle [y(t_k) * h_I(t_k)]^2 \rangle \end{aligned} \quad (5.109)$$

where

$$h_I(t) = \begin{cases} 0 & t < -\tau \\ 1/\tau & -\tau \leq t \leq 0 \\ 0 & t > 0 \end{cases} \quad (5.110)$$

In other words, the true variance $I^2(\tau)$ can be expressed by convolving the frequency noise $y(t)$ by a function $h_I(t)$ that represents the basic measurement of one sample \bar{y}_k . The convolution integral above, therefore, represents the output of a hypothetical filter with impulse response $h_I(t)$ receiving an input signal $y(t)$. The true variance is the mean square value of this output signal.

Hence, the true variance can be also expressed in the frequency domain as the area under the spectral density of the signal output by this filter, as

$$I^2(\tau) = \int_0^\infty S_y(f) |H_I(f)|^2 df \quad (5.111)$$

where $S_y(f)$ is the one-sided PSD of $y(t)$ and $H_I(f)$ is the characteristic filter transfer function, i.e. the Fourier transform of $h_I(t)$, whose square magnitude is given by

$$|H_I(f)|^2 = \left(\frac{\sin \pi \tau f}{\pi \tau f} \right)^2 \quad (5.112)$$

The resulting integral relationship is then:

$$I^2(\tau) = \int_0^\infty S_y(f) \left(\frac{\sin \pi \tau f}{\pi \tau f} \right)^2 df \quad (5.113)$$

The impulse response $h_I(t)$ and the square magnitude of the transfer function $|H_I(f)|^2$ are plotted in Figures 5.15 and 5.16, respectively. Some limitations of the practical applicability of $I^2(\tau)$ do appear from the fact that the transfer function $H_I(f)$ is approximately equal to one for $\pi \tau f \ll 1$: the true variance is therefore very sensitive to low Fourier frequency components in $S_y(f)$. In particular, we note that $I^2(\tau) \rightarrow \infty$ if $S_y(f) \propto 1/f$, a very common kind of power-law noise (cf. Section 5.9).

Finally, please note that the above relationship between frequency-domain characterization $S_y(f)$ and time-domain characterization $I^2(\tau)$ cannot be reversed in a closed form, at least in most general cases.

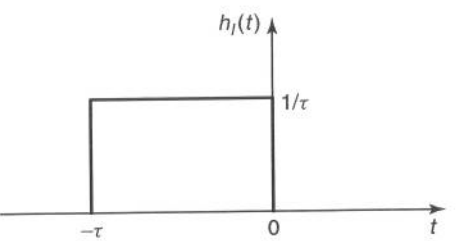


Figure 5.15. Impulse response $h_I(t)$ of the filter associated to the true variance

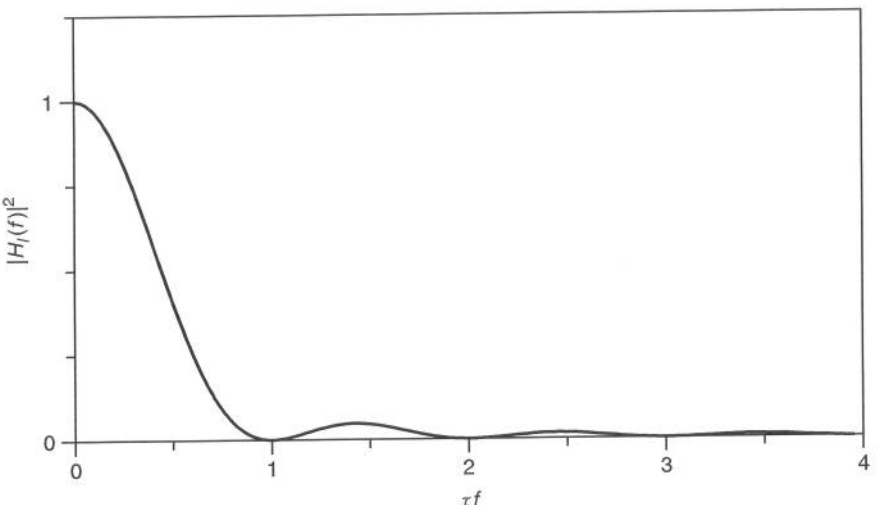


Figure 5.16. Square magnitude of the transfer function $H_I(f)$ associated with the true variance

5.8.10.2 *M*-Sample Variance of $y(t)$

Based on the M -sample variance definition given in Equation (5.87), for adjacent samples ($T = \tau$) it results [5.22]:

$$\langle \sigma_y^2(M, \tau, \tau) \rangle = \frac{M}{M-1} \int_0^\infty S_y(f) \left(\frac{\sin \pi \tau f}{\pi \tau f} \right)^2 \left[1 - \left(\frac{\sin M \pi \tau f}{M \sin \pi \tau f} \right)^2 \right] df \quad (5.114)$$

The key point is that the transfer function now behaves as proportional to f^2 for $M \pi \tau f \ll 1$, thus ensuring convergence of the integral even for kinds of power-law noise such as $S_y(f) \propto f^{-1}$ and $S_y(f) \propto f^{-2}$ (cf. Section 5.9).

5.8.10.3 Allan Variance

By letting $M = 2$ in Equation (5.114), we obtain directly the expression for the two-sample Allan variance $\sigma_y^2(\tau)$, as

$$\sigma_y^2(\tau) = \int_0^\infty S_y(f) \frac{2 \sin^4 \pi \tau f}{(\pi \tau f)^2} df \quad (5.115)$$

The impulse response $h_A(t)$ and the square magnitude of the transfer function

$$|H_A(f)|^2 = \frac{2 \sin^4 \pi \tau f}{(\pi \tau f)^2} \quad (5.116)$$

associated to the Allan variance are plotted in Figures 5.17 and 5.18, respectively.

Once again, we note that the relationship cannot be inverted for the most general cases. Moreover, the integral converges for all kinds of power-law noise (cf. Section 5.9) as in the previous case.

5.8.10.4 Modified Allan Variance

Directly from the definition of the modified Allan variance (5.93), we can derive the time-domain measurement filter impulse response $h_{MA}(n, t)$, plotted in Figure 5.19 for example in the case $n = 6$.

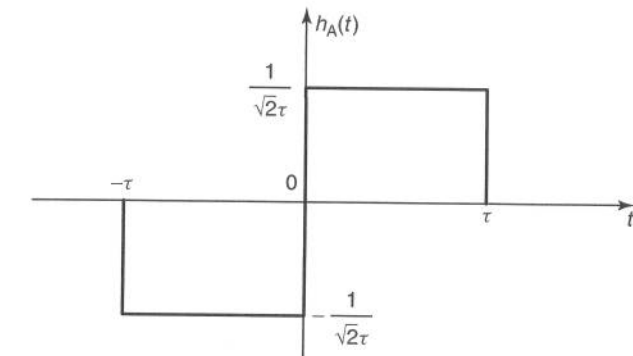


Figure 5.17. Impulse response $h_A(t)$ of the filter associated with the Allan variance

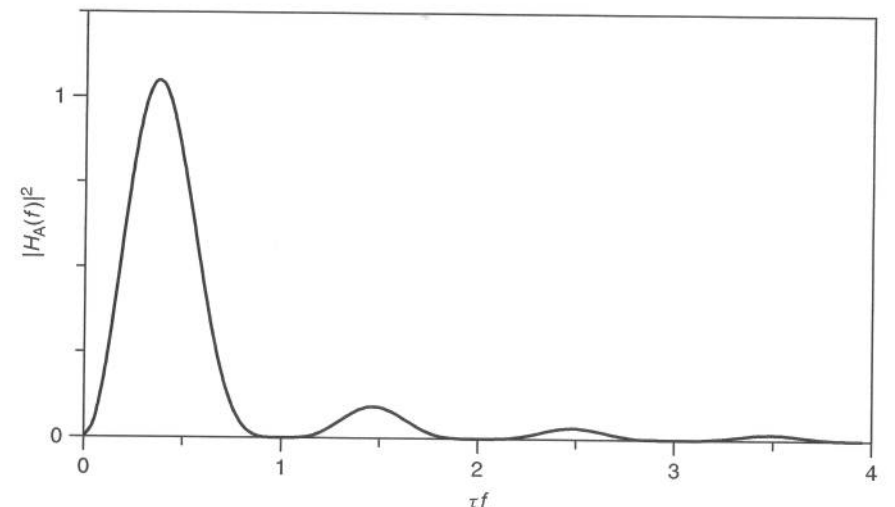


Figure 5.18. Square magnitude of the transfer function $H_A(f)$ associated with the Allan variance

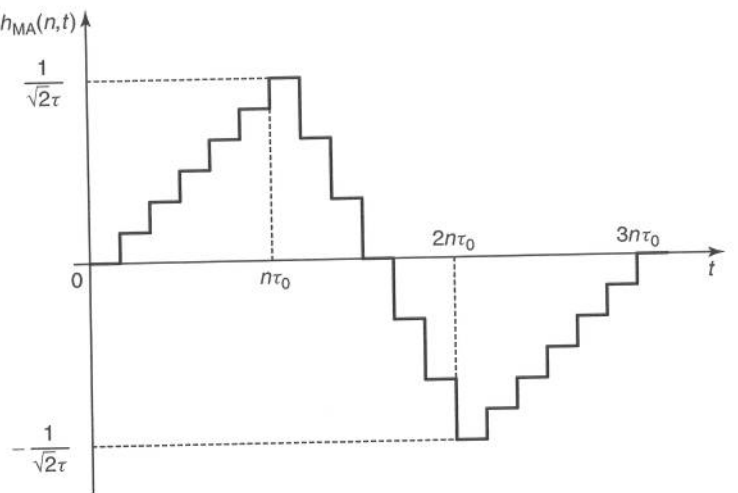


Figure 5.19. Impulse response $h_{MA}(n, t)$ of the filter associated with the modified Allan variance ($n = 6$)

The resulting integral relationship between the modified Allan variance and $S_y(f)$ results then

$$\text{Mod } \sigma_y^2(\tau) = \int_0^\infty S_y(f) \frac{2 \sin^6 \pi \tau f}{(n\pi \tau f)^2 \sin^2 \pi \frac{\tau}{n} f} df \quad (5.117)$$

The square magnitude of the characteristic transfer function $H_{MA}(n, f)$ is thus

$$|H_{MA}(n, f)|^2 = \frac{2 \sin^6 \pi \tau f}{(n\pi \tau f)^2 \sin^2 \pi \frac{\tau}{n} f} \quad (5.118)$$

The limit value of the transfer function $|H_{MA}(n, f)|^2$ for $n \rightarrow \infty$ and keeping $n\tau_0 = \tau$ constant is

$$\lim_{\substack{n \rightarrow \infty \\ n\tau_0 = \tau}} |H_{MA}(n, f)|^2 = 2 \frac{\sin^6 \pi \tau f}{(\pi \tau f)^4} \quad (5.119)$$

The square magnitude of the transfer function $|H_{MA}(n, f)|^2$ is plotted in Figure 5.20, for increasing values of the parameter n . It can be seen that the limit (5.119) is approached quickly for fairly low values of n .

5.8.10.5 Time Variance (TVAR)

Directly from the definition of TVAR (5.94) and from Equation (5.117), we can derive the following integral relationship between TVAR and $S_y(f)$

$$\sigma_x^2(\tau) = \int_0^\infty S_y(f) \frac{2 \sin^6 \pi \tau f}{3(n\pi f)^2 \sin^2 \pi \frac{\tau}{n} f} df \quad (5.120)$$

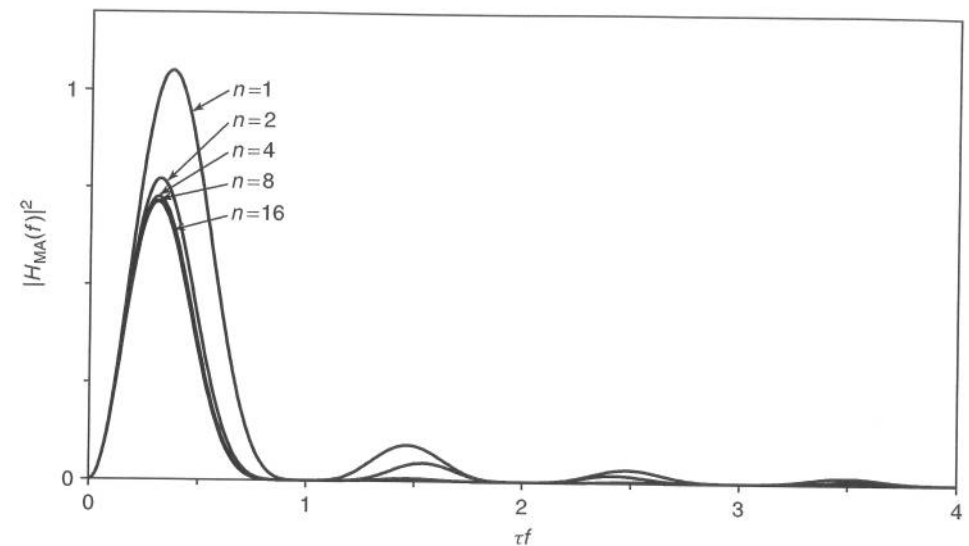


Figure 5.20. Square magnitude of the transfer function $H_{MA}(n, f)$ associated with the modified Allan variance for increasing values of the parameter n

5.8.10.6 Root Mean Square of the Time Interval Error (TIE_{rms})

If the only non-ideal component in the timing signal model (5.4) is the random frequency deviation $v_a(t)$, then the TIE_{rms} is directly linked to the classical variance of $y(t)$ by the relationship (5.97). Only under this assumption, the integral relationship between TIE_{rms} and $S_y(f)$ can be derived directly from (5.113) and results

$$\text{TIE}_{\text{rms}}(\tau) = \sqrt{\int_0^\infty S_y(f) \left(\frac{\sin \pi \tau f}{\pi f} \right)^2 df} \quad (5.121)$$

5.8.10.7 Maximum Time Interval Error (MTIE)

The Maximum Time Interval Error function MTIE(τ, T) is defined as the maximum peak-to-peak variation of TE in all the possible observation intervals τ within a measurement period T (cf. Equation (5.98)). Due to this peculiar nature of raw peak measure, it is not possible to translate to it from Fourier-frequency domain characterization by way of some integral relationship, based on a suitable transfer function, as we did for ‘normal’ stability quantities that are all based on some infinite time-averaging.

5.8.10.8 Transfer Functions as Tool to Define New Time-Domain Measures

Most time-domain quantities have been defined originally in the time domain, by defining a suitable processing of the time or frequency measurement samples. The shapes of the correspondent transfer functions have been derived from such definition in the time domain.

Nevertheless, the transfer function concept can be used also as a creative tool to define new quantities. According to this approach, a transfer function is first designed, depending on what kind of sensitivity is desired in the frequency domain. Then, the filter

impulse response is derived and hence the time-domain measurement data processing is determined.

As an example of this alternative approach, the Hadamard variance will be presented in the next section. Also other variances have been defined according to this approach (high-pass variance, band-pass variance, etc.). For further details, the reader is referred to the fundamental paper [5.22] by Rutman.

5.8.11 Hadamard Variance

The *Hadamard variance* has been developed by Baugh [5.43] to achieve high-resolution spectral analysis of $y(t)$ from measurements of \bar{y}_k . In other words, the goal was to estimate the frequency-domain quantity $S_y(f)$ from time-domain data provided by digital counters.

With this aim, the Hadamard variance was defined by designing a corresponding transfer function that contains a narrow main lobe, well suited for spectral analysis. The resulting time-domain definition is

$$\langle \sigma_H^2(M, T, \tau) \rangle = \langle (\bar{y}_1 - \bar{y}_2 + \bar{y}_3 - \cdots - \bar{y}_M)^2 \rangle \quad (5.122)$$

The Hadamard variance is thus calculated from groups of M samples \bar{y}_k , with $k = 1, 2, \dots, M$. Let us note, moreover, that the Allan variance $\sigma_y^2(\tau)$ is one-half times the Hadamard variance $\langle \sigma_H^2(M, T, \tau) \rangle$, with $M = 2$.

It has been shown that the Hadamard variance is related to $S_y(f)$ by the integral relationship

$$\langle \sigma_H^2(M, T, \tau) \rangle = \int_0^\infty S_y(f) \left(\frac{\sin \pi \tau f}{\pi \tau f} \right)^2 \left(\frac{\sin M \pi T f}{\cos \pi T f} \right)^2 df \quad (5.123)$$

The square magnitude of the characteristic transfer function $H_H(f)$ (i.e., the Fourier transform of the measurement sequence $h_H(t)$) is thus given by

$$|H_H(f)|^2 = \left(\frac{\sin \pi \tau f}{\pi \tau f} \right)^2 \left(\frac{\sin M \pi T f}{\cos \pi T f} \right)^2 \quad (5.124)$$

The measurement sequence $h_H(t)$ (for $M = 6$ and $T = \tau$) and the square magnitude of the transfer function $|H_H(f)|^2$ (for $M = 2, 4, 6$ and $T = \tau$) associated to the Hadamard variance are plotted in Figures 5.21 and 5.22, respectively. It can be seen that the transfer function exhibits a main lobe centred at the Fourier frequency $f_1 = 1/(2T)$. Its bandwidth decreases with increasing M .

Limitations and improvements for the practical use of the Hadamard variance are discussed in paper [5.22].

5.9 COMMON TYPES OF CLOCK NOISE

Experimental measurements on clocks may exhibit a variety of types of noise, either generated by physical processes intrinsic to the oscillator hardware or due to external phenomena. Such external phenomena include environmental perturbations, mechanical vibrations, residual ripples from the power supply, signal coupling via power supplies and ground paths, electromagnetic interference, etc.

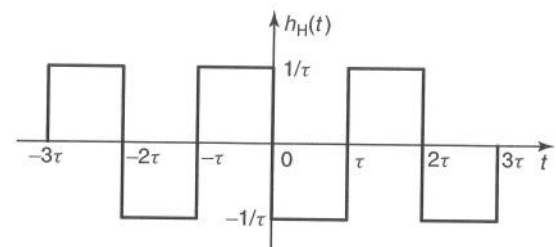


Figure 5.21. Impulse response $h_H(t)$ of the filter associated with the Hadamard variance ($M = 6$, $T = \tau$)

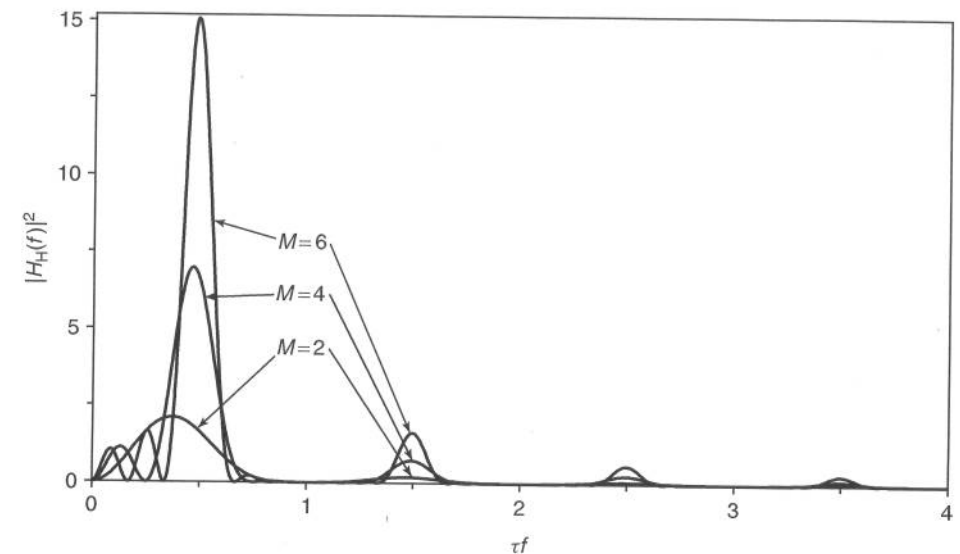


Figure 5.22. Square magnitude of the transfer function $H_H(f)$ associated with the Hadamard variance ($M = 2, 4, 6$ and $T = \tau$)

5.9.1 Power-Law Noise

In the frequency domain, the model most frequently used to represent the output phase noise measured on clocks is the so-called *power-law model*. In terms of the one-sided PSD of $x(t)$, such model is expressed by

$$S_x(f) = \begin{cases} \frac{1}{(2\pi)^2} \sum_{\alpha=-4}^0 h_{\alpha+2} f^\alpha & 0 \leq f \leq f_h \\ 0 & f > f_h \end{cases} \quad (5.125)$$

where the h_{-2} , h_{-1} , h_0 , h_{+1} and h_{+2} coefficients are device-dependent parameters¹⁵ and f_h is an upper cut-off frequency (*clock hardware bandwidth*), mainly depending on

¹⁵ The reason for the subscript $\alpha + 2$ (for $\alpha = -4, -3, -2, -1, 0$) is that, historically, the coefficients h_{-2} , h_{-1} , h_0 , h_{+1} and h_{+2} have been used in the definition of the power-law model, originally in terms of $S_y(f)$ (cf. Equation (5.76)).

low-pass filtering in the oscillator and in its output buffer amplifier. This clock upper cut-off frequency has been measured in the range 10–100 kHz in precision frequency sources [5.44].

In practice, the measurement set-up introduces a further low-pass filtering on the clock output noise, with cut-off frequency \hat{f}_h (*measurement hardware bandwidth*). The actual bandwidth of the $x(t)$ process measured is therefore limited by the smaller between f_h and \hat{f}_h . However, the measurement hardware bandwidth \hat{f}_h of modern stability measurement set-ups, based on digital measurement of the TE, can be in the range of MHz and above: this fact usually ensures that all the clock phase noise components are fully captured in performing measurements.

The five noise types of the power-law model are: *White Phase Modulation* (WPM) for $\alpha = 0$, *Flicker Phase Modulation* (FPM) for $\alpha = -1$, *White Frequency Modulation* (WFM) for $\alpha = -2$, *Flicker Frequency Modulation* (FFM) for $\alpha = -3$ and *Random Walk Frequency Modulation* (RWFM) for $\alpha = -4$. All the stability quantities defined in the previous sections are sensitive, according to different laws, to the presence of these noises in the timing signal (see e.g. [5.2][5.22][5.31]).

According to this model in the frequency domain, when the PSD $S_x(f)$ is plotted on a log–log diagram, a broken line made of straight segments is approximately obtained, one per noise type and each having slope equal to the corresponding power α (see Figure 5.23).

In the time domain, on the other hand, the random realizations of the noise process of each single type exhibit characteristic trends, which could be even recognized at a glance by an experienced eye. To give an idea, Figures 5.24(a) through 5.24(e) show sample realizations of TE, each affected respectively by one of the five types of power-law noise. Each realization was obtained by numerical simulation of the power-law model (5.125), according to the value of α specified.

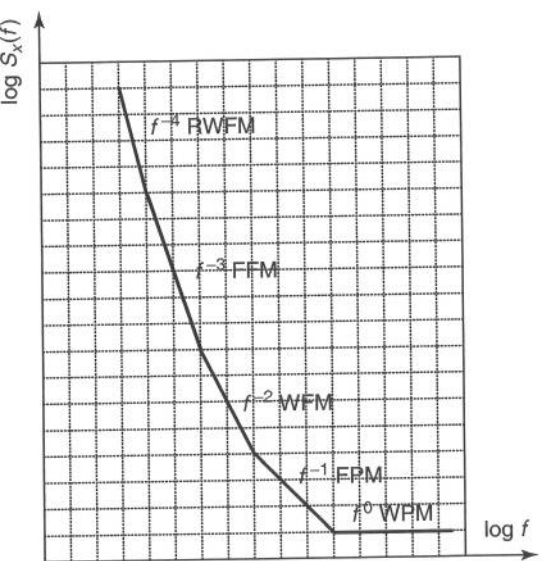


Figure 5.23. PSD $S_x(f)$ obeying the power-law model plotted on a log–log diagram

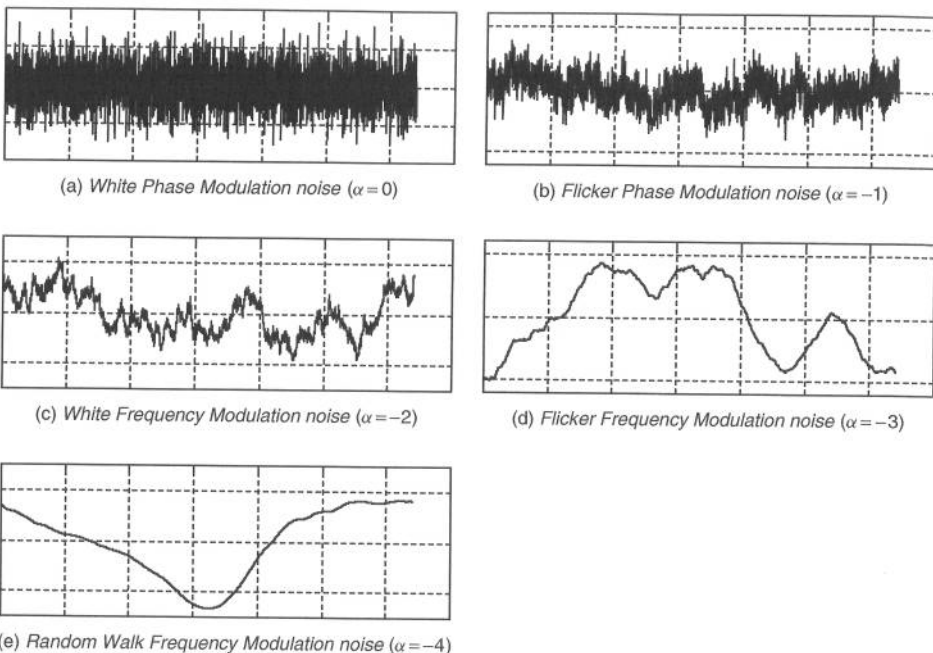


Figure 5.24. Sample realizations of the TE random process featuring the five types of power-law noise. (Reproduced from [5.40], ©1997 IEEE, by permission of IEEE)

First, in order to simulate WPM ($\alpha = 0$) noise, two white and uniformly distributed pseudo-random sequences of length $N = 2^{13} = 8192$ were generated. Then, applying a well-known transformation formula [5.45], one white Gaussian pseudo-random sequence of the same length was obtained, thus approximating a WPM noise. Spectral shaping was accomplished by filtering repeatedly in the Fourier domain the WPM ($\alpha = 0$) noise sequence through integrators of fractional order $-\alpha/2$ [5.46], having transfer function $H_{-\alpha/2}(f) = K(j2\pi f)^{\alpha/2}$, to generate the FPM ($\alpha = -1$), WFM ($\alpha = -2$), FFM ($\alpha = -3$) and RWFM ($\alpha = -4$) noise sequences according to the power-law model (5.125).

It is evident how TE realizations become smoother as we proceed from WPM to FPM, WFM, FFM and RWFM noise. This is obvious, as increasingly more power is concentrated at lower frequencies ($S_x(f) \propto f^{-\alpha}$).

The WFM noise has spectrum proportional to $1/f^2$. By remembering a well-known property of power spectra, it is therefore integral of a WPM noise, whose spectrum is constant. Actually, looking at the simulation procedure outlined above, the WFM noise realization in Figure 5.24(c) is the integral of the WPM noise plotted in Figure 5.24(a). In the same way, the RWFM noise realization in Figure 5.24(e) is the integral of the WFM noise plotted in Figure 5.24(c).

Then, what are then the flicker noise realizations plotted in Figures 5.24(b) and 5.24(d)? They were obtained by filtering the noise realizations plotted in Figures 5.24(a) and 5.24(c) by a transfer function of the form $H(f) = K(j2\pi f)^{-1/2}$. In the Fourier-frequency domain, it comes easy to say that such a transfer function corresponds to a *one-half order* integrator (it is less obvious to define such an operator in the time domain) [5.46]. Actually, a visual inspection of the waveforms plotted in Figures 5.24(b) and 5.24(d) may

lead to say that these processes are really something *in the middle* between the processes obtained by regular single and double integration.

These five power-law noise types may be due to different physical causes [5.25] and, on a particular oscillator, they may all be recognized or some may not. The main features and the supposed origin of each of the five types of power-law noise will be now summarized in brief.

- *Random Walk Frequency Modulation (h_{-2}/f^4)*. Difficult to measure as close to the carrier (the ideal timing signal). It is mostly ascribed to environmental effects: if RWFN noise dominates, then we may suppose that frequent perturbations like mechanical shocks or temperature variations cause random shifts in the oscillation frequency.
- *Flicker Frequency Modulation (h_{-1}/f^3)*. The causes of this type of noise are not fully understood, but they are mostly ascribed to the physical resonance mechanism of an active oscillator or to phenomena in the control electronic devices. FFM noise is commonly recognized in high-quality oscillators, but can be hidden by WFM or PFM noise in lower-quality oscillators.
- *White Frequency Modulation (h_0/f^2)*. It is a type of noise commonly recognized in passive-resonator frequency standards, which are based on a slave oscillator (mostly a quartz) locked to a resonance of another device. Caesium-beam and rubidium standards feature a dominant WFM noise.
- *Flicker Phase Modulation (h_1/f)*. Although it may be related to a physical resonance mechanism of the oscillator, it is mostly added by noisy electronics, especially in the output amplification stages and in the frequency multipliers.
- *White Phase Modulation (h_2)*. It has little to do with the clock resonance mechanism, but it is mainly added by noisy electronics. In the past, this type of noise was often negligible in high-quality clocks, featuring very low-noise output stages. Nowadays, conversely, clocks based on digital control electronics (such as the Digital PLLs, DPLLs) became very common, especially in telecommunications. This fact made the WPM noise the most commonly found in telecommunications measurements. WPM noise in DPLLs is due to the quantization error in the phase-lock loop, which produces a broadband white noise in the output timing signal. Moreover, WPM is the test-bench background noise caused by the trigger and quantization errors of time counters in the digital measurement of TE.

5.9.2 Periodic Noise

Although the power-law model proved very general and suitable for describing most measurement results, yet other types of noise may result in experimental measurements. Periodic noises are quite common. They may be typically caused by:

- interference from 50/60 Hz AC power line;
- diurnal and seasonal variations of temperature, which can affect the output frequency of the oscillator under test or much more frequently the signal propagation speed, for example on long copper cable lines (*diurnal* and *annual wander*);

- sensitivity to acoustic or mechanical vibrations;
- intrinsic phenomena such as special frequency control algorithms in DPLLs.

Periodic noise is revealed in frequency-domain measurement results as a series of spikes (ideally, lines at discrete frequencies) in the noise power spectrum. In time-domain measurement results, as it will be better shown later, periodic noise appears as ripples on the measured quantity. Examples of real measurement results featuring periodic noise will be shown in Section 5.10.3.

5.9.3 Background White Phase Noise Due to Trigger and Quantization Errors

Recently, time-domain measurement techniques based on digital time counters have become very common. Actually, in telecommunications, all standard measures are based on such instrumentation. A digital time counter is an instrument able to measure the elapsed time between two events (*start* and *stop trigger events*). This is achieved by incrementing a counter register with a very high and stable reference frequency (as it will be explained in Chapter 7, tricks like Vernier interpolation allow to improve the measurement resolution).

A *trigger event* typically consists of detecting an electric signal $V(t)$ going over some threshold V_{thr} on the input channel. Actually, the time instant t_{tr} in which the threshold is exceeded is recognized with some error ε_{tr} , due to the uncertainty ΔV_{thr} in the detection of the threshold level, as shown in Figure 5.25. The resulting error ε_{tr} is then called *trigger error*. It can be reduced by increasing the $V(t)$ signal slope around the threshold level. For this reason, it is always advisable to perform measurements on square wave signals rather than on sine waves.

Moreover, the measure of the time interval between the start and stop trigger events, obtained by reading the counter register, is affected by some *quantization error*, depending on instrumentation resolution.

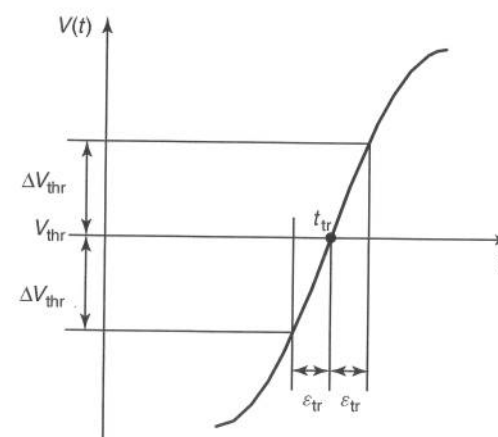


Figure 5.25. Error in recognizing the trigger-event time instant

Both trigger and quantization errors are revealed in measurement results as a background white noise. Therefore, WPM background noise is always experienced whenever time error is measured by a time counter, whereas WFM background noise is experienced if frequency measurements are carried out. Such background noise should be carefully evaluated before performing measurements on clocks.

Experimental Results

An example of real measurement results featuring background white noise due to trigger and quantization errors is provided in Figures 5.26 through 5.28. The measurement procedure is fully detailed in Appendix 7A. In short, the background noise of the measurement set-up was measured by splitting the 2.048 MHz reference timing signal and by feeding it directly into the time counter input ports. A sequence of $N = 96\,700$ samples of TE was acquired, with sampling period $\tau_0 \cong 37$ ms and over a measurement interval $T = 3600$ s. Then, ADEV and MADEV were computed with the standard estimators of Equations (5.104) and (5.105). The PSD $S_x(f)$ was computed (neglecting a multiplicative factor) through the Fast Fourier Transform (FFT) periodogram technique with triangular-shape data windowing, while the autocovariance function $C_x(\tau)$ was evaluated (again neglecting a multiplicative factor) as inverse transform of the PSD for $\tau \geq 0$ and mirrored copy for $\tau < 0$.

This background noise proves a pure WPM broadband noise: the ADEV and MADEV curves in Figure 5.26 are straight lines with slopes of τ^{-1} and $\tau^{-3/2}$ respectively, in perfect accordance with the theory (cf. Section 5.10.1), while the autocovariance $C_x(\tau)$ plotted in Figure 5.28 for $|\tau| \leq 10$ s features a $\delta(\tau)$ spike¹⁶ at $\tau = 0$.

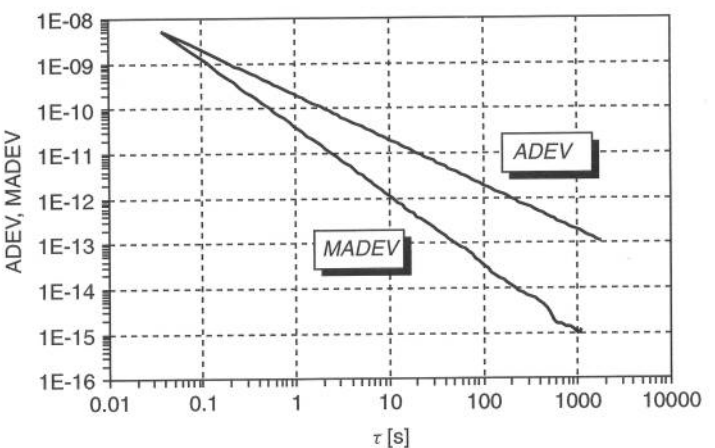


Figure 5.26. Measurement results featuring background WPM noise due to trigger and quantization errors—ADEV(τ) and MADEV(τ) ($N = 96\,700$, $\tau_0 \cong 37$ ms, $T = 3600$ s). (Reproduced from [5.32], ©1997 IEEE, by permission of IEEE)

¹⁶The spike has width really limited to the central sample $C_x(0)$. For the sake of precision, the first numerical values are $C_x(0) = 6.3 \times 10^{-6}$, $C_x(\pm\tau_0) = -6.8 \times 10^{-8}$, $C_x(\pm 2\tau_0) = 8.3 \times 10^{-8}$, $C_x(\pm 3\tau_0) = -3 \times 10^{-8}$, $C_x(\pm 4\tau_0) = 3.2 \times 10^{-8}$, $C_x(\pm 5\tau_0) = -1.8 \times 10^{-8}$, etc.

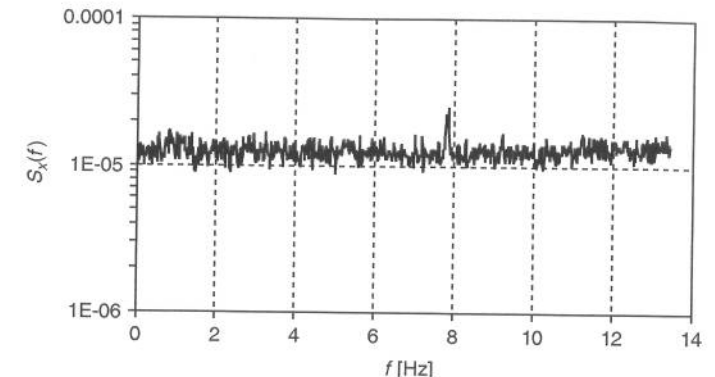


Figure 5.27. Measurement results featuring background WPM noise due to trigger and quantization errors—PSD estimate $S_x(f)$ ($N = 96\,700$, $\tau_0 \cong 37$ ms, $T = 3600$ s)

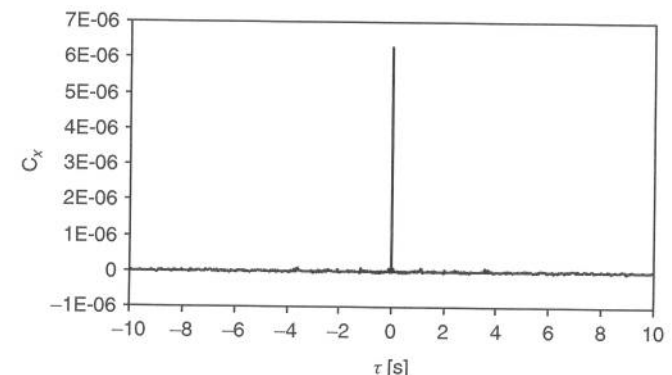


Figure 5.28. Measurement results featuring background WPM noise due to trigger and quantization errors—autocovariance function $C_x(\tau)$ ($N = 96\,700$, $\tau_0 \cong 37$ ms, $T = 3600$ s). (Reproduced from [5.32], ©1997 IEEE, by permission of IEEE)

5.10 BEHAVIOUR OF THE TIME-DOMAIN STABILITY QUANTITIES: AUTONOMOUS CLOCKS

The time-domain stability quantities defined in the previous sections reveal, with their particular behaviour, the presence of the different types of phase and frequency impairments on the signal under measurement. In this section, the effects of power-law noise, of frequency offset and drift and of periodic noise at the output of an autonomous clock are discussed. The characteristic trends of time-domain quantities for each type of such impairments are shown, thus allowing to properly interpret time-domain measurement results.

5.10.1 Power-Law Noise

Power-law noise has been previously defined in the frequency domain on the PSD $S_x(f)$ by the expression (5.125). Equivalent definitions can be given for other PSDs too, provided relationships such as those in Equation (5.76).